PROCEEDINGS OF SPIE

SPIEDigitalLibrary.org/conference-proceedings-of-spie

Liver surface reconstruction for image guided surgery

Congcong Wang, Faouzi Alaya Cheikh, Mounir Kaaniche, Ole Jakob Elle

Congcong Wang, Faouzi Alaya Cheikh, Mounir Kaaniche, Ole Jakob Elle, "Liver surface reconstruction for image guided surgery," Proc. SPIE 10576, Medical Imaging 2018: Image-Guided Procedures, Robotic Interventions, and Modeling, 105762H (13 March 2018); doi: 10.1117/12.2297398

SPIE.

Event: SPIE Medical Imaging, 2018, Houston, Texas, United States

Downloaded From: https://www.spiedigitallibrary.org/conference-proceedings-of-spie on 1/10/2019 Terms of Use: https://www.spiedigitallibrary.org/terms-of-use

Liver surface reconstruction for image guided surgery

Congcong Wang[a], Faouzi Alaya Cheikh[a], Mounir Kaaniche[b], and Ole Jacob Elle[c,d]

[a]Norwegian Colour and Visual Computing Lab, Norwegian University of Science and Technology, Norway.
[b]L2TI-Institut Galilée, Université Paris 13, Sorbonne Paris Cité, Villetaneuse, France.
[c]The Intervention Centre, Oslo University Hospital, Oslo, Norway.
[d]The Department of Informatics, University of Oslo, Oslo, Norway.

ABSTRACT

In image guided surgery, stereo laparoscopes have been introduced to provide a 3D view of the organs during the laparoscopic intervention. This stereo video could possibly be used for other purposes other than simple viewing: such as depth estimation, 3D rendering of the scene and 3D organ modeling. This paper aims at reconstructing 3D liver surface based on stereo vision technique. The estimated surface of the liver can later be used for registration to preoperative 3D model constructed from MRI/CT scans. For this purpose, we resort to a variational disparity estimation technique by minimizing a global energy function over the entire image. More precisely, based on the gray level and gradient constancy assumptions, a data term and a local as well as a non-local smoothness terms are defined to build the cost function. The latter is minimized, by using an appropriate optimization technique, to estimate the disparity map. In order to reduce the disparity search range and the influence of noise, the global variational approach is performed on the coarsest level of the multi-resolution pyramidal representation of the stereo images. Then the obtained low-resolution disparity map is up-sampled with a modified joint bilateral filtering method to the original scale. In vivo liver datasets with ground truth is difficult to obtain, so the proposed method is evaluated quantitatively on two cardiac phantom datasets from Hamlyn Center achieving an accuracy of about 2.2 mm for *heart1* and 2.1 mm for *heart2*. Reconstructed points up to 97% for *heart1* and 100% for *heart2* are obtained. Qualitative validation on in vivo porcine procedure's liver datasets has shown that our proposed method can estimate the untextured surfaces geometry well.

Keywords: surface reconstruction, variational, optimization, disparity up-sampling, stereo laparoscope, image guided surgery, liver.

1. INTRODUCTION

In the past decade, with the technological advances in laparoscopic devices, medical imaging and the demand for minimally invasive approaches have led to an increase in the number of laparoscopic resections.[1] On one hand, laparoscopic liver resection provides great benefits to patients, but on the other hand it increases the operation difficulty because of the limited field of view, poor depth perception and lack of the sense of touch. The technological advances in medical imaging and computing over the last twenty years enabled the use of image-based navigation systems in surgery. These systems, ultimately based on image pre-processing, tracking, visualization and 3D modeling techniques, increase the ability of the surgeon to perform surgery safely and accurately. In order to provide a 3D view of the organ for the surgeons intra-operatively, stereo laparoscopes have been introduced in image guided surgery. This can also be used to compute the depth information[2,3] of the organ or its surface by computer vision techniques which can be used to register to or update the preoperative 3D model constructed from MRI/CT scans.[4] This technology does not require additional hardware comparing to structured light or Time-of-Flight (ToF) based techniques.[5]

Stereo vision based surgical navigation has been developed for decades, as well as heart surface and abdominal soft tissue surface reconstruction.[6–10] Devernay *et al.*[6] present a dense stereo reconstruction method by using

Further author information:
E-mail: congcong.wang@ntnu.no, Telephone: +47 47731808

Medical Imaging 2018: Image-Guided Procedures, Robotic Interventions, and Modeling, edited by Baowei Fei, Robert J. Webster III, Proc. of SPIE Vol. 10576, 105762H · © 2018 SPIE
CCC code: 1605-7422/18/$18 · doi: 10.1117/12.2297398

Downloaded From: https://www.spiedigitallibrary.org/conference-proceedings-of-spie on 1/10/2019
Terms of Use: https://www.spiedigitallibrary.org/terms-of-use

normalized cross correlation and a hardware implementation which is regarded as the first work for minimally invasive surgery.[11] Later, some works are presented for the motion tracking of beating heart or the respiration of lung where the deformation is from physiological motion: a parametric surface description is proposed in[7] to overcome the difficulties of homogeneous texture for the smooth stereo reconstruction. In,[9] a Thin-Plate Spline model is proposed to represent the heart surface deformations. Another group of works is based on feature matching. Stoyanov *et al.*[8] propose a semi-dense reconstruction approach for robotic assisted minimally invasive surgery by first finding sparse matching features as seeds. Then a region growing method is used to propagate disparity information around the seeds. The performance of this reconstruction method can be influenced much by the initial feature points matching. Bernhardt *et al.*[12] use three criteria to discard outliers and only keep the most reliable matches. Their method shows robust results but has the risk of not enough matching points for a homogeneous surface. Penza *et al.*[13] apply a simple linear iterative clustering (SLIC) super-pixel algorithm for disparity refinement to improve the initial block matching method's matching percentage. Recently, in,[14] Totz *et al.* propose an approach for liver surgery. They adapted the feature matching propagation method proposed in[8] to a multi-resolution pyramid with a vertical propagation strategy. They present a faster but less accuracy results. Besides, global methods are also introduced for dense stereo reconstruction. A global convex optimization based method for real time dense reconstruction is presented in.[10] The proposed method overcomes the staircasing effect, but computing speed can be degraded for high resolution images as a result of the exhaustive search step of the approach. Allan *et al.*[15] regard the disparity estimation as a labeling problem on a Markov Random Field (MRF) and optimize it by a graph-cut algorithm which results in staircasing effect.

The lack of rich texture makes the feature matching process a challenging task in the context of laparoscopic liver resection. For this reason, instead of using a local disparity estimation method, a global approach is presented. In this paper, we first propose to use a variational disparity estimation method performed on a coarse pyramid level of the image. Such approach has the advantages of avoiding incorrect disparity estimation in texture-less areas and reducing the disparity search range as well as the error caused by noise. Besides, the continuity property of variational method can eliminate the undesired staircasing effect. Then, the generated low-resolution disparity map is up-sampled to the original scale.

This paper is organized as follows: Section 2 will introduce the proposed method. Section 3 will present the reconstruction results and Section 4 is the conclusion and future work.

2. METHOD

2.1 Variational Disparity Estimation Method

2.1.1 Cost function

In this part, the left image is selected as a reference image for the estimation of the disparity map. As there is not much occlusion during surgery if we only insert the camera into the human body, we could assume that the gray values and gradient of the two corresponding pixels in the left and right images are the same. The stereo images are undistorted and rectified, so search for stereo correspondences is performed only along the horizontal axis. The data term of our cost function is then given by:

$$\begin{aligned} E_{data}(d) &= |I_l(i,j) - I_r(i-d_{i,j},j)|^2 + \gamma|\bigtriangledown I_l(i,j) - \bigtriangledown I_r(i-d_{i,j},j)|^2 \\ &= \left|\mathbf{I}_l^{[k]}(i,j) - \mathbf{I}_r^{[k]}(i-d_{i,j},j)\right|^2, \end{aligned} \tag{1}$$

where E_{data} represents the data term, I_l and I_r are the left and right gray images respectively, $\bigtriangledown = (\partial_x, \partial_y)^\top$ is the spatial gradient operator, $d_{i,j}$ is the disparity value for pixel (i,j). $\mathbf{I}_l^{[k]}$ is the left multi-channel data term, defined as $\mathbf{I}_l^{[k]} = [I_l, \gamma I_{l_x}, \gamma I_{l_y}]^\top$, where I_{l_x}, I_{l_y} are the partial derivatives of I_l along the x and y dimensions respectively, k denotes the channels. γ is a scalar to adjust weights between the gray images and its gradient values in the data term. $\mathbf{I}_r^{[k]}$ is defined in a similar way as $\mathbf{I}_l^{[k]}$.

The organ surface is smooth, so we also can assume that the disparity is smoothly distributed:

$$E_s(d) = |\bigtriangledown d|^2. \tag{2}$$

Downloaded From: https://www.spiedigitallibrary.org/conference-proceedings-of-spie on 1/10/2019
Terms of Use: https://www.spiedigitallibrary.org/terms-of-use

We only consider the disparity value separately for every pixel locally so far, a non local regularization is a wise choice to improve the performance as presented in.[16] Therefore, we include a non-local term:

$$E_{nl} = \sum_{(i,j)\in\Omega_d} \sum_{(i',j')\in N_{i,j}} \left| d_{i,j} - d_{i',j'} \right|, \tag{3}$$

where $\Omega_d \in \mathbb{R}^2$ is the rectangular disparity map domain. $N_{i,j}$ represents the neighborhoods of pixel (i,j). This non-local term results in smoothness within a specific region defined by $N_{i,j}$ which could denoise the intermediate estimated disparity values and prevent outliers.[16]

Quadratic penalizer can be influenced too much by outliers, which would introduce large error for the registration part in a navigation system. So the Charbonnier penalty $\Psi(x^2) = \sqrt{x^2 + \epsilon^2}$ proposed in[17] is chosen here as it is differentiable and it is a robust convex function which shows promising performance in.[16,18,19]

The cost function is then defined as:

$$\begin{aligned} E(d) =& E_{data} + \lambda_s E_s + \lambda_{nl} E_{nl} \\ =& \Psi(\left| \mathbf{I}_l^{[k]}(i,j) - \mathbf{I}_r^{[k]}(i - d_{i,j}, j) \right|^2) + \lambda_s \Psi(|\bigtriangledown d|^2) + \lambda_{nl} \sum_{(i,j)\in\Omega_d} \sum_{(i',j')\in N_{i,j}} \left| d_{i,j} - d_{i',j'} \right|, \end{aligned} \tag{4}$$

where λ_s, λ_{nl} are parameters to adjust weights between data term, smooth term and non-local smooth term.

2.1.2 Optimization

The cost function in Eq. (4) is not convex, so instead of optimizing it directly, we use the heuristic median filtering strategy for the non-local term[16] and convex optimization approach for the other part.

The convex part of the cost function ($E_{data} + \lambda_s E_s$) can be solved by a linearization and fixed-point iteration method presented in,[18] in which a coarse to fine with warping strategy is used. Since the warping optimization approach is trying to build a linear system with two linearization steps, similarly to,[19] we do not process gray images and gradient part separately as presented in,[18] but use a multi-channel data term as shown in Eq. (1) for the purpose of a simple minimization implementation and a flexible definition of the data term. Then it is possible to include more channels in the multi-channel image $\mathbf{I}^{[k]}$ (for example the color value channels) without increasing the optimization complexity.

In,[16] the authors show that heuristic median filtering strategy can be regarded as a way of energy minimization of a cost function with a non-local term. Therefore, we apply median filtering for every intermediate estimated disparity. More details can be found in[16,18] about the warping based optimization and median filtering strategy.

2.2 Disparity Up-sampling

After applying the global variational method on the image at the highest scale of the pyramid, the resulting low-resolution disparity map d is up-sampled to the next pyramid level by a modified joint bilateral filter presented in[20] through Eq. (5). This process is repeated iteratively until we reach the original size of the image.

$$\widetilde{d}_p = \frac{1}{k'_p} \sum_{q_\downarrow \in N} I_{q_\downarrow} f(\|p_\downarrow - q_\downarrow\|) \cdot [\alpha(\Delta N) g(\|\widetilde{\mathbf{I}}_p - \widetilde{\mathbf{I}}_q\|) + (1 - \alpha(\Delta N)) h(\|d_{p_\downarrow} - d_{q_\downarrow}\|)], \tag{5}$$

where $\widetilde{d}_p$ is the upsampled disparity map. f, g, h are Gaussian functions, $\|\cdot\|$ is the Euclidean norm, $\widetilde{\mathbf{I}}$ is the high resolution color image which corresponds to the left (resp. right) image when the disparity is estimated with respect to the left (resp. right) view. d is the low resolution disparity map. p and q are pixels in the high resolution image, and $p_\downarrow$ and $q_\downarrow$ are pixels in the low resolution image/disparity map. N represents the spatial neighborhood around $p_\downarrow$. We propose to define ΔN as the mean gradient magnitude in pixel neighborhood N while it is the difference between the maximum and minimum value of N in.[20] k'_p is a normalizing factor. α is a blending function which is defined as a sigmoid function (Eq. (6)), where τ is defined as the mean gradient magnitude for the whole disparity map d here and ϵ can be defined experimentally.

$$\alpha(\triangle N) = \frac{1}{1 + e^{-\epsilon \cdot (\triangle N - \tau)}}. \tag{6}$$

Downloaded From: https://www.spiedigitallibrary.org/conference-proceedings-of-spie on 1/10/2019
Terms of Use: https://www.spiedigitallibrary.org/terms-of-use

A high α value makes the filter similar to a bilateral up-sampling filter which preserves the edges. If an area is geometrically smooth but has a high value in the distance measurement on the color image (e.g. there are different colors on the same surface), a bilateral filter will cause texture copy error, so a low α value is needed to give higher weight to the disparity term $h(\|d_{p\downarrow} - d_{q\downarrow}\|)$ and lower weight to the color image term $g(\|\widetilde{\mathbf{I}}_p - \widetilde{\mathbf{I}}_q\|)$.[20]

Once the up-sampled disparity maps are obtained for both the left ($\widetilde{d}_l$) and right images ($\widetilde{d}_r$), a simple left and right consistency check is performed (Eq. (7)): for the disparity of a particular pixel (i, j), the value is set to invalid if the differences between $\widetilde{d}_l$ and $\widetilde{d}_r$ are higher than a predefined threshold value th.

$$\hat{d}_l(i,j) = \begin{cases} \widetilde{d}_{inv}, & if \left|(\left|\widetilde{d}_l(i,j)\right| - \left|\widetilde{d}_r(i - \widetilde{d}_l(i,j), j)\right|)\right| > th \\ \widetilde{d}_l(i,j), & otherwise \end{cases}, \tag{7}$$

Then the surface is generated by using the standard triangulation technique.

3. EXPERIMENTAL RESULTS

The algorithm is validated on the publicly available datasets[8,21,22] from Hamlyn Centre Laparoscopic / Endoscopic Video Dataset [*] quantitatively and qualitatively. This research is mainly devoted to image guided liver resection, as the lack of ground truth for in vivo liver datasets, cardiac phantom datasets *heart1* and *heart2*[8,21] are used for quantitative evaluation and in vivo porcine liver datasets[22] are used for qualitative evaluation. The implementation is benefited from a source code provided by Sun *et al.*. [†16] The input gray images are preprocessed by highboost filtering to sharpen the detail of the original images:[23]

$$\tilde{I}_v = I_v + k(I_v - \bar{I}_v), \tag{8}$$

where I_v is the original left/right gray image, $\bar{I}_v$ denotes the blurred image by a Gaussian filter and $k = 3$.

3.1 Quantitative Evaluation

In this evaluation, the ground truth disparity and depth maps of the two stereo sequences (*heart1* and *heart1*) are generated by CT data through manual registration. The stereo image pairs are undistorted and rectified by the provided camera calibration parameters before perform the disparity estimation and reconstruction. The main parameters used for the two datasets are: $\gamma = 50$, $\lambda_s = 30$, median filter size is $[5, 5]$, number of warping per pyramid level is 3 and linearization per warping is 5. Upsampling step's window size is 3, ϵ is 0.5, up-sampling factor is 4, which means the up-sampled disparity size is 4 times larger than the coarse level disparity's size.

Prior to the accuracy evaluation of the proposed method, we choose the region of interest by removing the dark background. An intensity threshold is used to remove the dark background (15 %). Besides, the region of interest should be visible in both of the right and left images, so we crop the left image by 45 pixels at the left side of the image. Fig. 1 shows an example of the original images (Fig. 1 (a) and (c)) and cropped images (Fig. 1 (b) and (d)) used for evaluation for datasets *heart1* and *heart2*, the pixels marked with blue color are cropped and not included for evaluation.

As the ground truth disparity maps are given for the original images, our estimated disparity values are obtained from the rectified images, we can not compare the disparity values directly. Therefore, a standard triangulation method is applied to calculate 3D point cloud for each pixel. The estimated depth values are then compared to the rectified ground truth depth. We should note that the triangulation step will introduce error. Mean Absolute Error (MAE, given by Eq. (9)) between the ground truth depth y and the estimated one $\hat{y}$ is computed as a metric of accuracy.

$$MAE = \frac{1}{H \times W} \sum_{(i,j)\in\Omega} |\hat{y}(i,j) - y(i,j)|, \tag{9}$$

[*] http://hamlyn.doc.ic.ac.uk/vision/

[†] http://cs.brown.edu/~dqsun/research/index.html#pubs/

Downloaded From: https://www.spiedigitallibrary.org/conference-proceedings-of-spie on 1/10/2019
Terms of Use: https://www.spiedigitallibrary.org/terms-of-use

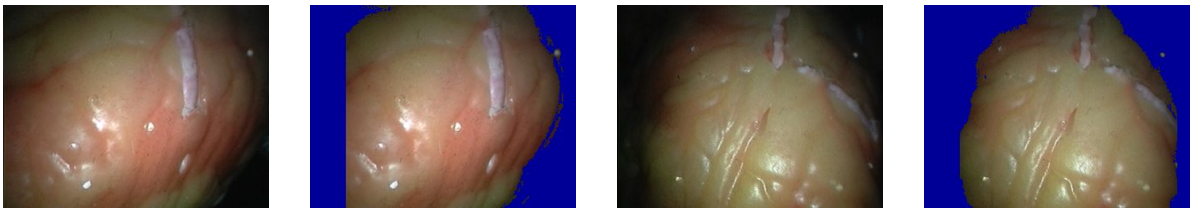

(a) (b) (c) (d)

Figure 1. The region used for evaluation (the left images selected from the first frame of the two datasets are shown as an example here). (a) the original image from *heart1*; (b) the cropped image from *heart1*, the pixels marked with blue color are cropped; (c) the original image from *heart2*; (d) the cropped image from *heart2*, the pixels marked with blue color are cropped.

where H and W present the height and the width of the depth maps, Ω is the rectangular depth map domain and $y(i,j)$ indicates the depth value for a pixel (i,j). Percentage of matched pixels (% Match) is also used for evaluation. As described in,[13] % Match is defined as the ratio between the numbers of reconstructed points and pixels of the region of interest of the image. Our proposed method is compared with a quasi-dense method (QuasiDense)[8] which is proposed for robotic assisted minimally invasive surgery and it performs well in terms of accuracy in the comparison results presented in.[14] Besides, a fast cost-volume filtering method (FCVF)[24] is also chosen for comparison which showed its potential for endoscopic scene reconstruction in the work presented in.[25]

In Table 1, mean and standard deviation of MAE and % Match for the first 500 frames of *heart1* and *heart2* are reported. Our method has the lowest mean MAE error and highest % Match values. Although the MAE values of our method and the QuasiDense are quite similar, our approach has higher % Match than QuasiDense. An example of the obtained results is shown in Fig. 2, it can be seen that our approach produces smooth disparity map close to the ground truth.

Table 1. MAE (mm) and % Match for phantom datasets *heart1* and *heart2*.

	heart1		*heart2*	
Methods	MAE(mm)	% Match	MAE(mm)	% Match
Proposed Method	$\mathbf{2.16 \pm 0.65}$	$\mathbf{97.25 \pm 1.13}$	$\mathbf{2.14 \pm 0.83}$	$\mathbf{99.96 \pm 0.11}$
QuasiDense[8]	2.33 ± 0.61	78.64 ± 2.00	2.26 ± 0.52	80.64 ± 1.87
FCVF[24]	4.43 ± 0.81	95.96 ± 1.57	4.21 ± 1.20	88.92 ± 2.38

3.2 Qualitative Evaluation

Fig. 3 shows the reconstructed porcine liver surface from three different datasets captured by different stereo laparoscopes. Surface estimation of those images is a quite challenging problem. Our method benefits from the global estimation and the fill-in effect of variational methods which can have dense results. QuasiDense gives sparse results for *dataset1* and *dataset3* with lots of noises, and fails to find proper match between left and right images for *dataset2* as shown in Fig. 3 (c). The results of FCVF are quite noisy as shown in Fig. 3 (d). On the contrary of these two methods, the proposed one provides smooth and dense reconstructions in all cases. But whether the estimated geometry fulfills the requirement for registration or not needs to be addressed further by more accurate evaluation strategy.

4. CONCLUSION

In this paper, a dense liver surface reconstruction approach from stereo laparoscopic images is presented to overcome lack of features problem in liver surgery. Experimental results show that our reconstruction method can accurately estimate the surface geometry which will be used in following registration step for image guided

Downloaded From: https://www.spiedigitallibrary.org/conference-proceedings-of-spie on 1/10/2019
Terms of Use: https://www.spiedigitallibrary.org/terms-of-use

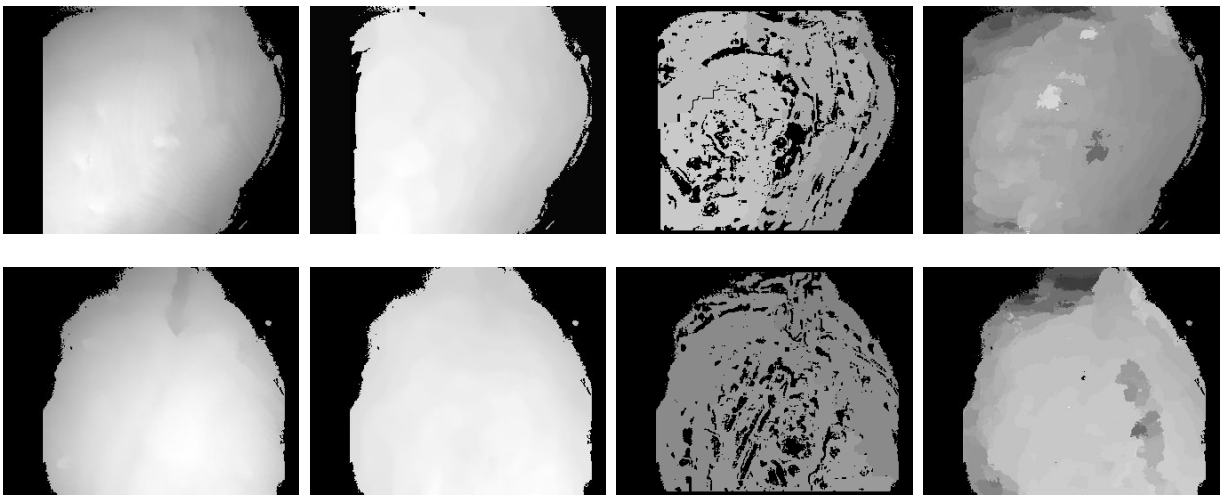

(a) (b) (c) (d)

Figure 2. Example of the disparity results for the first frame of *heart1* and *heart2*. (a) Ground truth disparity map; (b) disparity map estimated by our proposed method; (c) disparity map estimated by QuasiDense;[8] (d) disparity map estimated by FCVF.[24]

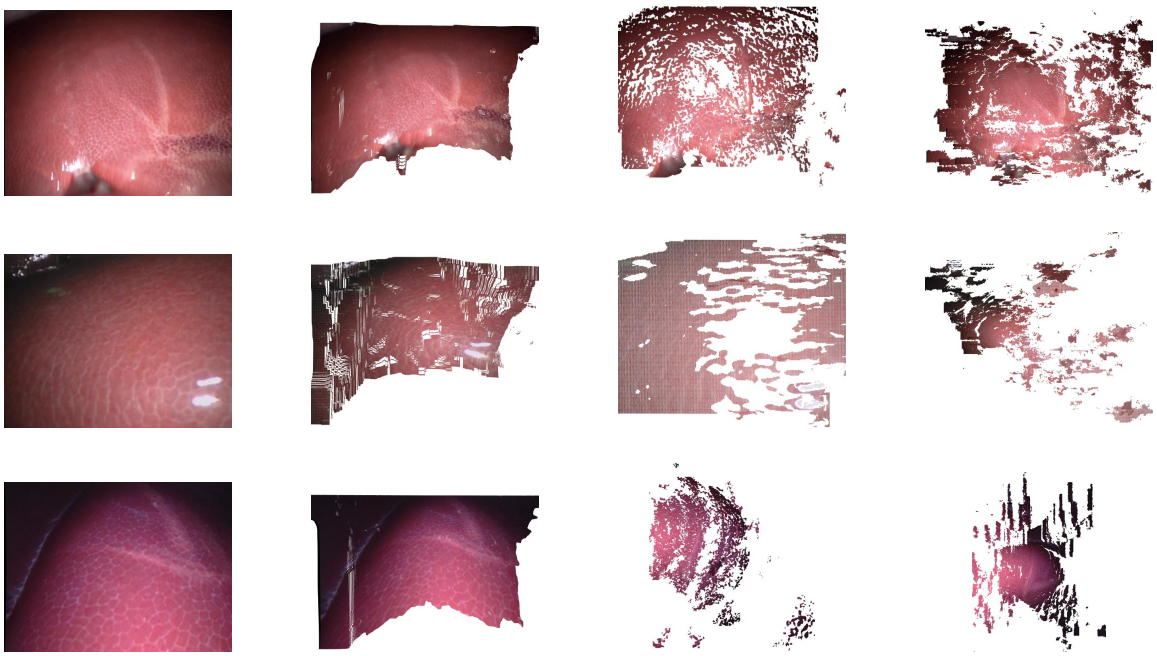

(a) (b) (c) (d)

Figure 3. Example of surface estimation results for in vivo porcine liver datasets. (a) Undistorted and rectified left image; (b) surface estimated by our proposed method; (c) surface estimated by QuasiDense;[8] (d) surface estimated by FCVF.[24]

Downloaded From: https://www.spiedigitallibrary.org/conference-proceedings-of-spie on 1/10/2019
Terms of Use: https://www.spiedigitallibrary.org/terms-of-use

liver resection system. Further improvements could be achieved in the future by focusing on the following investigations: pre-processing of the stereo laparoscopic images, introducing more robust channels and non-local term in the data term part, and taking into account edge information as well as occlusion in the energy function.

ACKNOWLEDGMENTS

The authors would like to acknowledge Yu Fan, Ahmed Kedir Mohammed for the valuable discussions and Ivar Farup for mathematical explanation. This work is funded by the Research Council of Norway through project no. 247689 IQ-MED: Image Quality enhancement in MEDical diagnosis, monitoring and treatment.

REFERENCES

[1] Nguyen, K. T., Marsh, J. W., Tsung, A., Steel, J. J. L., Gamblin, T. C., and Geller, D. A., "Comparative benefits of laparoscopic vs open hepatic resection: a critical appraisal," *Archives of surgery* **146**(3), 348–356 (2011).

[2] Kaaniche, M., Gaetano, R., Cagnazzo, M., and Pesquet-Popescu, B., "Disparity estimation techniques," in [*Emerging Technologies for 3D Video: Creation, Coding, Transmission and Rendering*], 81–101, Wiley Eds (2013).

[3] Scharstein, D. and Szeliski, R., "A taxonomy and evaluation of dense two-frame stereo correspondence algorithms," *International journal of computer vision* **47**(1-3), 7–42 (2002).

[4] Palomar, R., Cheikh, F. A., Edwin, B., Beghdadi, A., and Elle, O. J., "Surface reconstruction for planning and navigation of liver resections," *Computerized Medical Imaging and Graphics* **53**, 30–42 (2016).

[5] Bernhardt, S., Nicolau, S. A., Soler, L., and Doignon, C., "The status of augmented reality in laparoscopic surgery as of 2016," *Medical image analysis* **37**, 66–90 (2017).

[6] Devernay, F., Mourgues, F., and Coste-Manière, È., "Towards endoscopic augmented reality for robotically assisted minimally invasive cardiac surgery," in [*International Workshop on Medical Imaging and Augmented Reality*], 16–20, IEEE (2001).

[7] Lau, W., Ramey, N., Corso, J., Thakor, N., and Hager, G., "Stereo-based endoscopic tracking of cardiac surface deformation," in [*International Conference on Medical Image Computing and Computer-Assisted Intervention*], 494–501, Springer (2004).

[8] Stoyanov, D., Scarzanella, M. V., Pratt, P., and Yang, G.-Z., "Real-time stereo reconstruction in robotically assisted minimally invasive surgery," in [*International Conference on Medical Image Computing and Computer-Assisted Intervention*], 275–282, Springer (2010).

[9] Richa, R., Bó, A. P., and Poignet, P., "Towards robust 3d visual tracking for motion compensation in beating heart surgery," *Medical Image Analysis* **15**(3), 302–315 (2011).

[10] Chang, P.-L., Stoyanov, D., Davison, A. J., and Edwards, P. E., "Real-time dense stereo reconstruction using convex optimisation with a cost-volume for image-guided robotic surgery," in [*International Conference on Medical Image Computing and Computer-Assisted Intervention*], 42–49, Springer (2013).

[11] Maier-Hein, L., Mountney, P., Bartoli, A., Elhawary, H., Elson, D., Groch, A., Kolb, A., Rodrigues, M., Sorger, J., Speidel, S., and Stoyanov, D., "Optical techniques for 3d surface reconstruction in computer-assisted laparoscopic surgery," *Medical image analysis* **17**(8), 974–996 (2013).

[12] Bernhardt, S., Abi-Nahed, J., and Abugharbieh, R., "Robust dense endoscopic stereo reconstruction for minimally invasive surgery," in [*International MICCAI Workshop on Medical Computer Vision*], 254–262, Springer (2012).

[13] Penza, V., Ortiz, J., Mattos, L. S., Forgione, A., and De Momi, E., "Dense soft tissue 3d reconstruction refined with super-pixel segmentation for robotic abdominal surgery," *International Journal of Computer Assisted Radiology and Surgery* **11**(2), 197–206 (2016).

[14] Totz, J., Thompson, S., Stoyanov, D., Gurusamy, K., Davidson, B. R., Hawkes, D. J., and Clarkson, M. J., "Fast semi-dense surface reconstruction from stereoscopic video in laparoscopic surgery," in [*International Conference on Information Processing in Computer-Assisted Interventions*], 206–215, Springer (2014).

[15] Allan, M., Kapoor, A., Mewes, P., and Mountney, P., "Non rigid registration of 3d images to laparoscopic video for image guided surgery," in [*International Workshop on Computer-Assisted and Robotic Endoscopy*], 109–116, Springer (2015).

Downloaded From: https://www.spiedigitallibrary.org/conference-proceedings-of-spie on 1/10/2019
Terms of Use: https://www.spiedigitallibrary.org/terms-of-use

[16] Sun, D., Roth, S., and Black, M. J., "A quantitative analysis of current practices in optical flow estimation and the principles behind them," *International Journal of Computer Vision* **106**(2), 115–137 (2014).

[17] Bruhn, A., Weickert, J., and Schnörr, C., "Lucas/kanade meets horn/schunck: Combining local and global optic flow methods," *International Journal of Computer Vision* **61**(3), 211–231 (2005).

[18] Brox, T., Bruhn, A., Papenberg, N., and Weickert, J., "High accuracy optical flow estimation based on a theory for warping," *Computer Vision-ECCV 2004* , 25–36 (2004).

[19] Sand, P. and Teller, S., "Particle video: Long-range motion estimation using point trajectories," *International Journal of Computer Vision* **80**(1), 72–91 (2008).

[20] Chan, D., Buisman, H., Theobalt, C., and Thrun, S., "A noise-aware filter for real-time depth upsampling," in [*Workshop on Multi-camera and Multi-modal Sensor Fusion Algorithms and Applications-M2SFA2*], (2008).

[21] Pratt, P., Stoyanov, D., Visentini-Scarzanella, M., and Yang, G.-Z., "Dynamic guidance for robotic surgery using image-constrained biomechanical models," *Medical Image Computing and Computer-Assisted Intervention–MICCAI 2010* , 77–85 (2010).

[22] Mountney, P., Stoyanov, D., and Yang, G.-Z., "Three-dimensional tissue deformation recovery and tracking," *IEEE Signal Processing Magazine* **27**(4), 14–24 (2010).

[23] Gonzalez, R. C. and Woods, R. E., [*Digital Image Processing (3rd Edition)*], Prentice-Hall, Inc., Upper Saddle River, NJ, USA (2006).

[24] Hosni, A., Rhemann, C., Bleyer, M., Rother, C., and Gelautz, M., "Fast cost-volume filtering for visual correspondence and beyond," *IEEE Transactions on Pattern Analysis and Machine Intelligence* **35**(2), 504–511 (2013).

[25] Luo, X., McLeod, A. J., Jayarathne, U. L., Pautler, S. E., Schlacta, C. M., and Peters, T. M., "Towards disparity joint upsampling for robust stereoscopic endoscopic scene reconstruction in robotic prostatectomy," in [*SPIE Medical Imaging*], 97860Q–97860Q, International Society for Optics and Photonics (2016).

Downloaded From: https://www.spiedigitallibrary.org/conference-proceedings-of-spie on 1/10/2019
Terms of Use: https://www.spiedigitallibrary.org/terms-of-use